

Anti-inflammatory and Antioxidative Effects of Tetrahedral DNA Nanostructures via the Modulation of Macrophage Responses

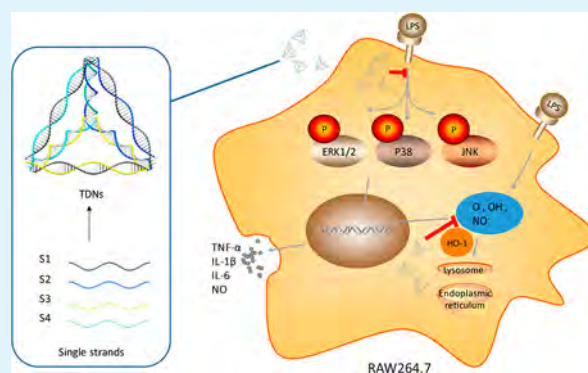
Qi Zhang,[†] Shiyu Lin,[†] Sirong Shi,[†] Tao Zhang,[†] Quanquan Ma,[†] Taoran Tian,[†] Tengfei Zhou,[†] Xiaoxiao Cai,[†] and Yunfeng Lin^{*,†} 

[†]State Key Laboratory of Oral Diseases, West China Hospital of Stomatology, Sichuan University, Chengdu 610041, People's Republic of China

Supporting Information

ABSTRACT: Tetrahedral DNA nanostructures (TDNs) are a new type of nanomaterials that have recently attracted attention in the field of biomedicine. However, the practical application of nanomaterials is often limited owing to the host immune response. Here, the response of RAW264.7 macrophages to TDNs was comprehensively evaluated. The results showed that TDNs had no observable cytotoxicity and could induce polarization of RAW264.7 cells to the M1 type. TDNs attenuated the expression of NO IL-1 β (interleukin-1 β), IL-6 (interleukin-6), and TNF- α (tumor necrosis factor- α) in LPS-induced RAW264.7 cells by inhibiting MAPK phosphorylation. In addition, TDNs inhibited LPS-induced reactive oxygen species (ROS) production and cell apoptosis by up-regulating the mRNA expression of antioxidative enzyme heme oxygenase-1 (HO-1). The findings of this study demonstrated that TDNs have great potential as a novel theranostic agent because of their anti-inflammatory and antioxidant activities, high bioavailability, and ease of targeting.

KEYWORDS: TDNs, anti-inflammatory activity, antioxidative activity, cell polarization, MAPK signaling pathway



1. INTRODUCTION

Advances in nanotechnology have brought about a shift in the application of several biofunctional molecules to imaging tracers and therapeutic agents.¹ Biofunctional molecules such as peptides, proteins, and traditional chemotherapy drugs can be loaded onto or connected with nanoparticles, such as quantum dots, gold nanoparticles, and DNA nanostructures.^{2–6} The dosages and corresponding side effects of these drugs can be reduced owing to the nanoparticle properties, whereas the properties and effects of targets can be optimized.⁷ Among various kinds of nanostructures, DNA nanostructures are deemed as ideal and promising materials because of their designability in structure and sequence diversity. Multifunctional and sophisticated DNA nanocomposites such as tetrahedral DNA nanostructures, aptamer nanobeacons, and DNA-based logic functions can be fabricated.^{3,4} Tetrahedral DNA nanostructures (TDNs), one of the most promising DNA nanostructures, have recently been considered as potential biomaterials for extensive applications.^{8–11} TDNs are self-assembled by four highly specific and programmable DNA single chains (ssDNA).^{12–14} The design of ssDNA allows precise complementary base pairing, sequence designability, and specific hybridization of complementary functional sequences.^{15,16} Different from ssDNA, TDNs could enter mammalian cells without lipofection and remain intact in the cytoplasm for at least 48 h, which are important properties for

applications in drug delivery and the control of its activity in the cell.¹⁷ As an easily modified nanostructure, TDNs have been applied to transport the immunostimulant CpG into cells to induce immunostimulatory effects.¹⁸ Ge et al. combined TDNs and hybridization chain reaction amplification to achieve ultrasensitive microRNA detection.¹⁹ Moreover, TDNs and siRNAs are able to self-assemble targeted DNA/siRNA nanoparticles for delivery *in vivo*, resulting in stable gene silencing.¹⁶ In our previous studies, we have reported that TDNs play important roles in promoting cell migration,²⁰ maintaining the chondrocyte phenotype,²¹ and promoting stem cell osteogenesis.²²

Owing to these broad roles, TDNs can be widely used in the field of biomedicine. However, when applied to organisms, the immune system defends against invasion of foreign particles. In case of immune rejection, excessive production of inflammatory cytokines and mediators can lead to severe systemic complications, substantially limiting the *in vivo* use of TDNs. Therefore, a comprehensive understanding of the immunoregulatory effects of TDNs will be important for determining its safety and efficacy. When administered, nanoparticles are very likely to come into contact with macrophages in the alveoli,

Received: November 24, 2017

Accepted: January 4, 2018

Published: January 4, 2018

liver, spleen, lymph nodes, and other organs.²³ Thus, RAW264.7 cells, which participate in the innate immune response,²⁴ were used as a model to evaluate cellular response to TDNs.

To the best of our knowledge, this is the first study that comprehensively analyzes immunological effects of TDNs, including the reaction to cell polarization and cell apoptosis, as well as their anti-inflammatory and antioxidative stress effects. In the inflammatory response, mitogen-activated protein kinase (MAPK) signaling has important effects on the regulation of pro-inflammatory cytokines and mediators. To elucidate the molecular and cellular pathways by which TDNs regulate oxidative stress and inflammation, Western blotting was used to examine the activation of the MAPKs (ERK1/2, p38, and JNK) in macrophages. These detection approaches could help indicate whether the TDNs have good biocompatibility and immunomodulatory effects. Furthermore, our results may form a basis for the potential application of TDNs in the development of anti-inflammatory and antioxidant drugs.

2. MATERIALS AND METHODS

2.1. Preparation of TDNs. TDNs were synthesized as described previously.²¹ Prefabricated single-strands in TM buffer underwent denaturation for 10 min at 95 °C followed by pairing for least 30 min at 4 °C.¹⁰

2.2. Characterization of TDNs. Polyacrylamide gel electrophoresis (PAGE) and transmission electron microscopy (TEM) were employed for verifying successful fabrication and analyzing relevant characteristics. Dynamic light scattering by Zetasizer Nano ZS90 (Malvern Instrument Ltd., Malvern, UK) was applied to examine the basic characteristics of TDNs, such as zeta potential and average size.

2.3. Culture, Induction, and Treatment. High-glucose Dulbecco's modified Eagle's medium (DMEM) supplemented with 10% (v/v) FBS was used to culture RAW 264.7 cells. The cells were divided into four groups for the following experiments: (1) blank control, (2) RAW264.7 cells induced by lipopolysaccharides (LPS; 1 µg/mL, lipopolysaccharide from *Escherichia coli* O55:B5, Sigma-Aldrich, St. Louis, Missouri, USA), (3) RAW264.7 cells incubated with TDNs (250 nM), and (4) RAW264.7 cells preincubated with TDNs (250 nM) for 1 h and then treated with LPS (1 µg/mL).

2.4. Cell Counting. Cells were seeded in a 96-well plate (2×10^4 /well) and incubated with 100 µL of fresh growth medium overnight. The next day, the medium was exchanged with high-glucose DMEM supplemented with 1% FBS. After 2 h of starvation, cells were treated with TDNs or LPS (1 µg/mL) for 12 and 24 h. CCK-8 solution²⁵ was applied to the cells, and they were counted by measuring the absorbance at 450 nm.²⁶

2.5. Cellular Uptake of Cy5-loaded TDNs. Cellular uptake of TDNs was analyzed using flow cytometry. Briefly, cells were seeded in six-well plates (2×10^5 /well) with fresh growth medium for 24 h. Then, the medium was replaced with fresh high-glucose DMEM supplemented with 1% FBS. After 2 h of starvation, cells were preincubated with 250 nM Cy5-loaded TDNs (1.5 mL/well) and collected at 0.5, 1, 2, and 3 h. The cellular uptake at each time point was tested by a flow cytometer (FC500 Beckman, IL, USA).

2.6. Griess Assay. A Griess assay kit (Appligen, Beijing, China) was used for the detection of NO production. Macrophages (2×10^4 /well) were cultured in 96-well plates and preincubated with TDNs (0, 125, 250, 500 nM) for 1 h and then treated with LPS (0, 1 µg/mL) for 12, 24, and 48 h. Nitrite production was detected by measuring the absorbance at 540 nm. The results were determined using sodium nitrite as a standard, and then the level of NO in treated cells was calculated.

2.7. Immunofluorescence. The abundance of iNOS was detected by immunofluorescence. RAW264.7 cells (1×10^5 /well) were cultured in a six-well plate and preincubated with TDNs (0, 250 nM) for 1 h

and then treated with LPS (0, 1 µg/mL). After 12 h of treatment and incubation, cells underwent fixation in paraformaldehyde (4% (w/v)) for 15 min and Triton X-100 (0.5%) for 10 min.²⁷ Samples were blocked using 5% sheep serum for 1 h and then incubated with the primary antibody against iNOS (1:250, ab178945; Abcam, Cambridge, UK) at 4 °C overnight. Then, the samples were incubated with secondary antibody conjugated with fluorescence (1:500; Thermo Fisher Scientific, MA, USA) for 1 h. Phalloidine and DAPI were applied to stain the cytoskeleton and nuclei.^{28,29} Cell morphology was observed via confocal laser microscopy (Leica TCS SP8, Germany).

2.8. Quantitative PCR. RNA levels of iNOS, arginase, and heme oxygenase-1 (HO-1) were detected by quantitative PCR (q-PCR). The sequences of primer pairs are listed in Table 1. Briefly, total RNA

Table 1. Sequences of Forward and Reverse Primers of Selected Genes Designed for qPCR

| gene | | primer pairs |
|----------|---------|---------------------------------|
| arginase | forward | 5'-CAGAAGAATGGAAGAGTCAG-3' |
| | reverse | 5'-GGTGACTCCCTGCATATCTG-3' |
| HO-1 | forward | 5'-CAGGTGTCCAGGAGAAGGCTTT-3' |
| | reverse | 5'-TCTTCCAGGGCCGTGTAGAT-3' |
| β-actin | forward | 5'-TGGCTCCTAGCACCATGAA-3' |
| | reverse | 5'-CTCAGTAACAGTCCGCCTAGAAGCA-3' |
| iNOS | forward | 5'-CCTCCTCCACCCTACCAAGT-3' |
| | reverse | 5'-CACCCAAAGTGCTTCAGTCA-3' |

in RAWs was extracted by TRIzol (Thermo Fisher Scientific, MA, USA).^{30,31} A cDNA synthesis kit (MBI, Glen Burnie, MD, USA) was used to prepare cDNA. Target cDNA was amplified in ABI7900 according to following steps: 95 °C for 30 s, followed by 40 cycles (5 s at 95 °C followed by 34 s at 60 °C).^{32,33} A melting curve was applied to detect the presence of primer dimers and false priming.

2.9. Western Blotting. Expression of iNOS, ERK1/2, p-ERK1/2, p38, p-p38, JNK1/2/3, and p-JNK1/2/3 was examined by Western blotting. Samples were rinsed, and then, total proteins were harvested by whole cell lysis assay (KeyGen, Nanjing, China). Protein samples and loading buffer were mixed at a ratio of 4:1 and then boiled. Subsequently, 10% SDS-PAGE was performed to separate target proteins. The target proteins were transferred onto a PVDF membrane.³² After blocking in 5% BSA for 1 h, target membranes were incubated with anti iNOS (ab178945, 1:1000; Abcam, Cambridge, UK), ERK (ab184699, 1:1000; Abcam), p38 (ab32142, 1:1000; Abcam), JNK (ab179461, 1:1000; Abcam), p-ERK (ab201015, 1:1000; Abcam), p-p38(ab195049, 1:1000; Abcam), and p-JNK (ab124956, 1:1000; Abcam) primary antibodies overnight at 4 °C, followed by incubation with secondary antibodies (Beyotime, Shanghai, China) for 1 h. Subsequently, the membrane was washed with TBST, and detection was performed by using the Bio-Rad detection system.

2.10. ELISA. TNF-α, IL-1β, and IL-6 secretion was assayed using ELISA kits (Multi Sciences, China). Cells in six-well plates were divided into four groups: (1) blank control, (2) RAW264.7 cells treated with LPS (1 µg/mL), (3) RAW264.7 cells incubated with TDNs (250 nM), and (4) RAW264.7 cells preincubated with TDNs (250 nM) for 1 h and then induced by LPS (1 µg/mL). Supernatants were collected at 12 and 24 h.

2.11. Detection of ROS Level. Reactive oxygen species (ROS) were detected by the DCFH-DA assay. Briefly, after culturing the RAW264.7 cells in a six well plate for 24 h, the medium was replaced with fresh high-glucose DMEM supplemented with 1% FBS. After 2 h of starvation, cells were incubated with TDNs (0, 250 nM) for 1 h and then treated with LPS (0, 1 µg/mL). After incubation for 12 h, cells were incubated with DCFH-DA for 25 min followed by digestion and washed three times. Finally, the cells were suspended in 0.5 mL of PBS and analyzed by flow cytometry (FC500 Beckman, IL, USA). Results were analyzed by Flowjo software.

2.12. Measurement of Intracellular ROS Levels by Fluorescence Microscopy. Cells at a density of 1×10^5 /mL were seeded in six-well plates. After 24 h of culture, the medium was replaced with

Table 2. Base Sequence of Each Single-Stranded DNA (ssDNA)

| ssDNA | direction | base sequence |
|-------|-----------|---|
| S1 | 5'→3' | ATTTATCACCCGCCATAGTAGACGTATCACCAGGCAGTTGAGACGAACATTCTAAGTCTGAA |
| S2 | 5'→3' | ACATGCGAGGGTCCAATACCGACGATTACAGCTTGCTACACGATTACAGACTTAGGAATGTTTCG |
| S3 | 5'→3' | ACTACTATGGCGGGTGATAAAACGTGTAGCAAGCTGTAATCGACGGGAAGAGCATGCCCATCC |
| S4 | 5'→3' | ACGGTATTGACCCTCGCATGACTCAACTGCCTGGTGATACGAGGATGGGCATGCTCTTCCCG |

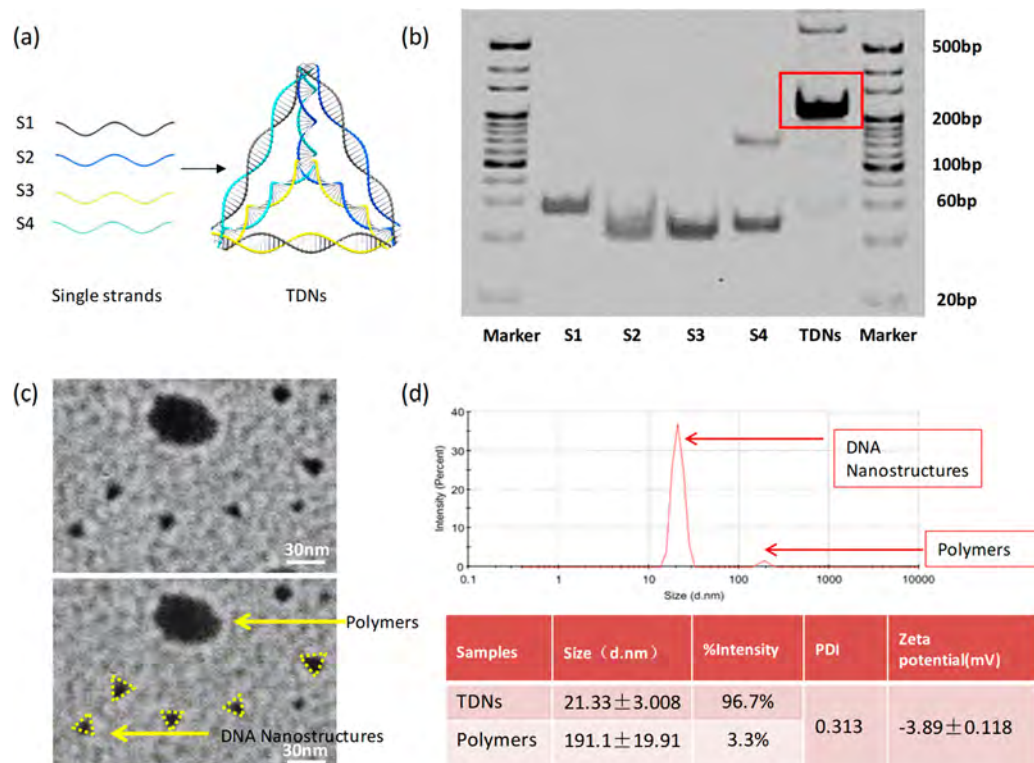


Figure 1. Synthesis and characterizations of TDNs. (a) A schematic illustration showing the composition of TDNs. (b) Polypropylene Acyl Amine Gel Electrophoresis (PAGE) analysis of the successful production of TDNs. (c) Transmission electron microscope (TEM) images of single TDNs and the polymers. (d) Size distribution and zeta potential test of TDNs. Data are presented as mean ± SD ($n = 4$).

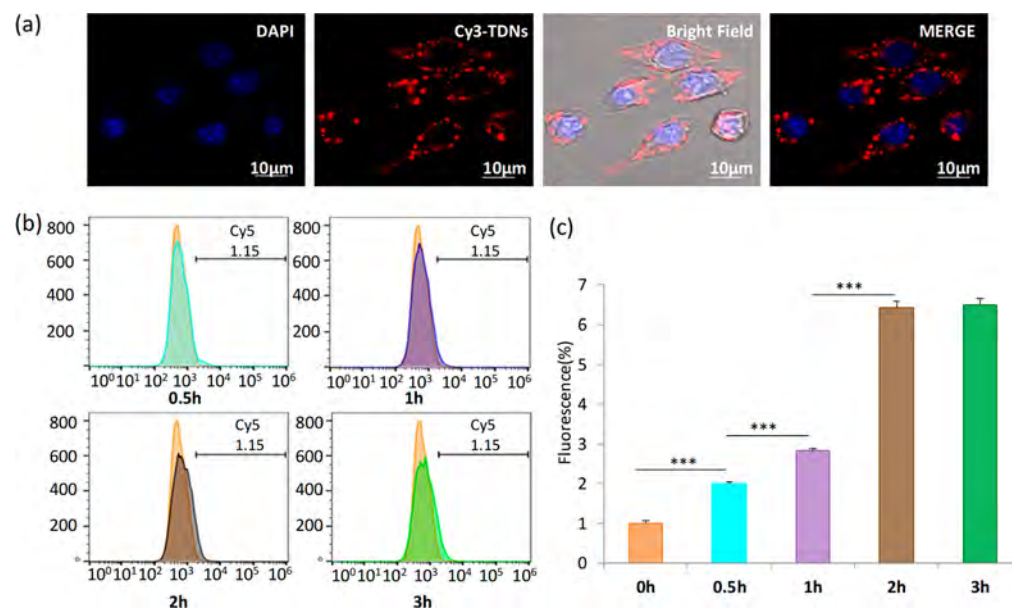


Figure 2. Cellular uptake of TDNs. (a) Reaction of Cy3-TDN (nucleus, blue; Cy3-TDNs, red). Scale bars are 10 μm . (b) Flow cytometric examination and analysis of cellular uptakes of Cy5-TDNs. (c) Semi-quantitative analysis of cellular uptake in flow cytometry. The uptake of TDNs increased significantly with the incubation time and reached saturation within 3 h. Data are presented as mean ± SD ($n = 4$).

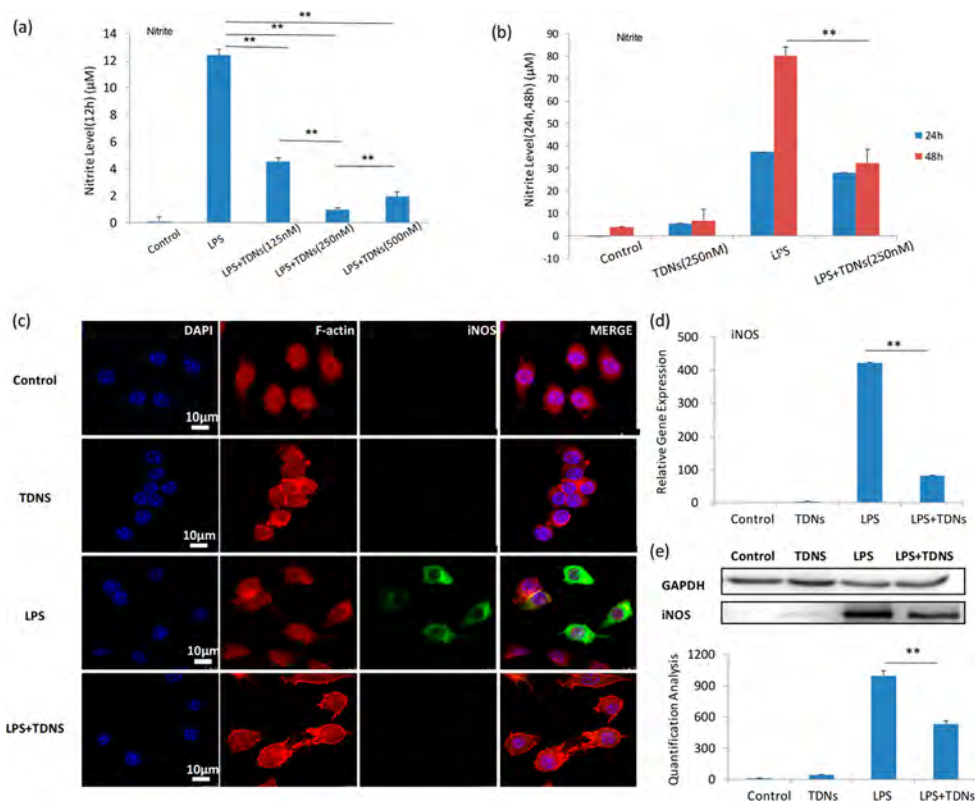


Figure 3. Influences of LPS and TDNs on production of NO and expression of iNOS. (a) Production of nitrite at 12 h after treatment of LPS and different concentration of TDNs. (b) Production of nitrite at 24 h and 48 h after treatment of LPS and 250 nM TDNs. (c) Immunofluorescent images of treated RAW264.7 cells (nucleus, blue; F-actin, red; iNOS, green). Scale bars are 10 μm . (d) Q-PCR analysis of the gene expression of iNOS. Data are presented as mean \pm SD ($n = 4$). (e) Western blot detection and quantification of iNOS. Data are presented as mean \pm SD ($n = 4$). Statistic differences are significant among the four groups ($p < 0.05$); we specially labeled the statistic difference between the LPS group and LPS TDNs group. Statistical analysis: * $p < 0.05$, ** $p < 0.01$.

fresh high-glucose DMEM supplemented with 1% FBS. After 2 h of starvation, cells were pretreated with TDNs (0, 250 nM) for 1 h and then treated with LPS (0, 1 $\mu\text{g}/\text{mL}$). After incubation for 12 h, samples were incubated with DCFH-DA for 25 min. Immunofluorescence images were obtained using a microscope.

2.13. Flow Cytometric Analysis of Cell Apoptosis. An Annexin V FITC apoptosis detection kit (KeyGEN, Jiangsu, China) was employed for cell apoptosis assay. In brief, RAW 264.7 cells were divided into two groups: (1) positive control, cells with 1 $\mu\text{g}/\text{mL}$ LPS, and (2) cells incubated with TDNs (250 nM) for 1 h and then with 1 $\mu\text{g}/\text{mL}$ LPS. Adherent cells were digested (without EDTA) and washed twice. Binding buffer (500 μL), 5 μL of Annexin V-FITC mix, and 5 μL of propidium iodide were added. Finally, the target samples were suspended in 0.5 mL of PBS and analyzed by flow cytometry (FC500 Beckman, IL, USA). Results were analyzed by the Summit 5.2 software.

2.14. Statistical Analysis. Experiments were performed independently four times. Statistical evaluation was performed by one-way ANOVA or t -test in SPSS 21.0 (IBM, Silicon Valley, USA). Multiple comparisons were done using an LSD test or Dunnett's t test.

3. RESULTS AND DISCUSSION

3.1. Synthesis and Characterization of TDNs. As shown in Table 2, TDNs were composed of equimolar amounts of four single-stranded DNA (ssDNA) molecules by base pairing (Figure 1a). The results of SDS-PAGE showed that TDNs were successfully self-assembled (Figure 1b). The morphology of TDNs was characterized by TEM (Figure 1c). On the basis of the TEM images, we observed triangular nanoparticles and some polymers. In addition, we studied the size and zeta

potential of TDNs via dynamic light scattering (Figure 1d). The average diameter of TDNs reached up to approximately 21.33 nm; moreover, numerous polymers formed during TDN synthesis. TDNs had a particle dispersion index (PDI) of 0.313, indicating that it is a moderate dispersed system. The DNA tetrahedron had a negatively charged surface of -3.89 ± 0.118 mV. In summary, we successfully prepared DNA nanostructures with similar size and surface potential for use in subsequent studies.

3.2. Cellular Uptake of TDNs. It is important to explore the uptake of nanoparticles for better understanding of their toxicity and functionality.³⁴ To track TDNs in RAW264.7 cells, we loaded the fluorescent dye Cy3 in one ssDNA. Cells were treated with Cy3-TDNs, and the uptake of TDNs was observed by confocal microscopy (Figure 2a). From the images, it was observed that a large number of Cy3-TDNs were stably maintained in the cytoplasm. Then, flow cytometry was applied to quantitatively analyze the uptake of TDNs by RAW264.7 cells at different time points (Figure 2b). RAW264.7 cells were incubated with Cy5-labeled TDNs and harvested at 0.5, 1, 2, and 3 h after treatment. As shown in Figure 2c, Cy5 fluorescence in macrophages increased significantly over time and reached saturation within 3 h. Single- and double-stranded DNA are usually plasma membrane-impermeable owing to their polyanionic properties. Naked oligodeoxynucleotides cannot be absorbed by cells and can be easily cleared by nucleases in the serum or cytoplasm.³⁵ Although the TDNs have a negatively charged surface, they have been demonstrated to easily penetrate through the cell membrane in the absence of

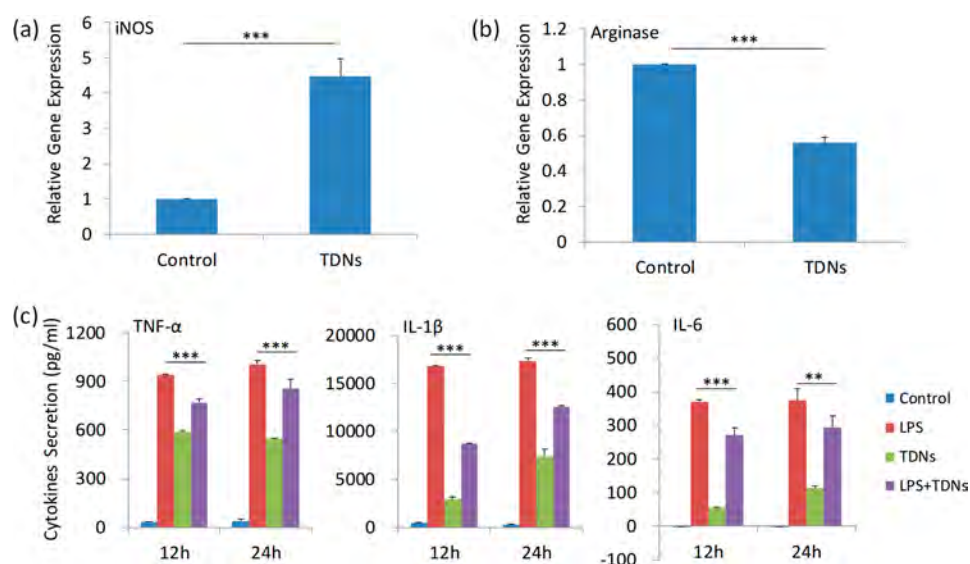


Figure 4. Macrophage polarization and inflammatory cytokines secretion. (a,b) Q-PCR analysis of gene expressions of iNOS and arginase. (c) ELISA detection of the inflammatory cytokines (TNF- α , IL-1 β , IL-6) secretion at 12 h and 24 h after treatment. Data are presented as mean \pm SD ($n = 4$). Statistical analysis: ** $p < 0.01$, *** $p < 0.001$. Statistic differences are significant among the four groups ($p < 0.05$); we specially labeled the statistic difference between the LPS group and LPS TDNs group.

a transfection agent, showing properties different from those of their linear counterparts.^{12,20,21,36} Liang et al. reported that TDNs were internalized by a caveolin-dependent pathway and transported to lysosomes in a microtubule-dependent manner.^{16,37} These results provide a basis for the possibility of targeted treatment approaches based on TDNs.

3.3. TDNs Decrease LPS-Induced NO Production. The immune system may possibly defend against invasion of foreign particles when TDNs would be applied to organisms. In the case of immune rejection, excessive production of inflammatory cytokines and mediators can lead to severe systemic complications, substantially limiting the *in vivo* use of TDNs. To investigate whether TDNs play a role in the inflammatory response, we treated RAW264.7 cells with LPS to establish an inflammatory response model. The production of NO, an inflammatory mediator, was examined by Griess assay. As indicated in Figure 3a, LPS stimulation caused a significant increase in NO content, whereas TDNs decreased NO production, particularly at the dose of 250 nM. When treated with TDNs only, the NO production level was very similar to that observed in the control group. Therefore, 250 nM is the optimal concentration for further investigations. We observed the release of NO at different time points and found that TDNs continued to exert an anti-inflammatory effect within 48 h (Figure 3b).

Notably, the biological effect of NO depends on its concentration and subtle changes in the concentration both inside and outside the cell. Under normal physiological conditions, small quantities of NO are beneficial to the body.³⁸ However, excessive production of NO in tissues can also cause tissue damage, malignancy, rheumatoid arthritis, and septic shock.³⁹ The above results suggested that TDNs could slightly promote the secretion of NO in noninflammatory cells. However, TDNs could resist the excessive production of NO in LPS-induced inflammation in RAW264.7 cells. It can be concluded that TDNs can significantly regulate the balance of NO production.

Endogenous NO is mainly derived from the conversion of L-arginine into L-citrulline and NO. Enzymes involved in this process include neuronal NO synthase (nNOS), endothelial NO synthase (eNOS), and inducible NO synthase (iNOS).^{40,41} The former two can be found in neurons and endothelial cells, respectively, while the latter is especially distributed in macrophages, hepatocytes, astrocytes, and smooth muscle cells in response to inflammatory mediators such as LPS and cytokines. Many recent advances have demonstrated that iNOS is responsible for inducible NO production.^{42,43} LPS treatment upregulates iNOS expression, thereby regulating the production of NO.^{44,45} Therefore, we further explored the effect of TDNs on iNOS expression (Figure 3c,d,e). Consistent with NO production, LPS induced the overexpression of the iNOS protein; however, TDNs attenuated this elevation. With respect to iNOS mRNA level, no significant difference could be found between control group and cells incubated with TDNs alone. These results suggested that TDNs inhibited NO production via iNOS transcriptional regulation and further downregulated the production of NO.

3.4. Macrophage Polarization Stimulated by TDNs. Macrophages are highly plastic and can be activated to M1/M2 subtypes depending on microenvironmental signals.⁴⁶ Activation of the M1 phenotype can be detected by the iNOS marker, and that of the M2 phenotype can be detected by the arginase marker. When macrophages undergo “classical” activation, i.e., M1 macrophages, they secrete various pro-inflammatory factors associated with secondary inflammation and are known as pro-inflammatory macrophages. When macrophages acquire the M2 phenotype, they secrete factors that contribute to tissue repair and are known as repair macrophages.

Therefore, the effect of TDNs on activation and polarization of macrophages through cell interaction was investigated by detecting the markers of macrophage polarization. On the basis of the results of q-PCR, RAW264.7 cells pretreated with TDNs exhibited greater expression of the pro-inflammatory cytokine, iNOS, than that of the untreated cells (Figure 4a). In contrast, the M2 marker *Arginase* showed reduced expression in the

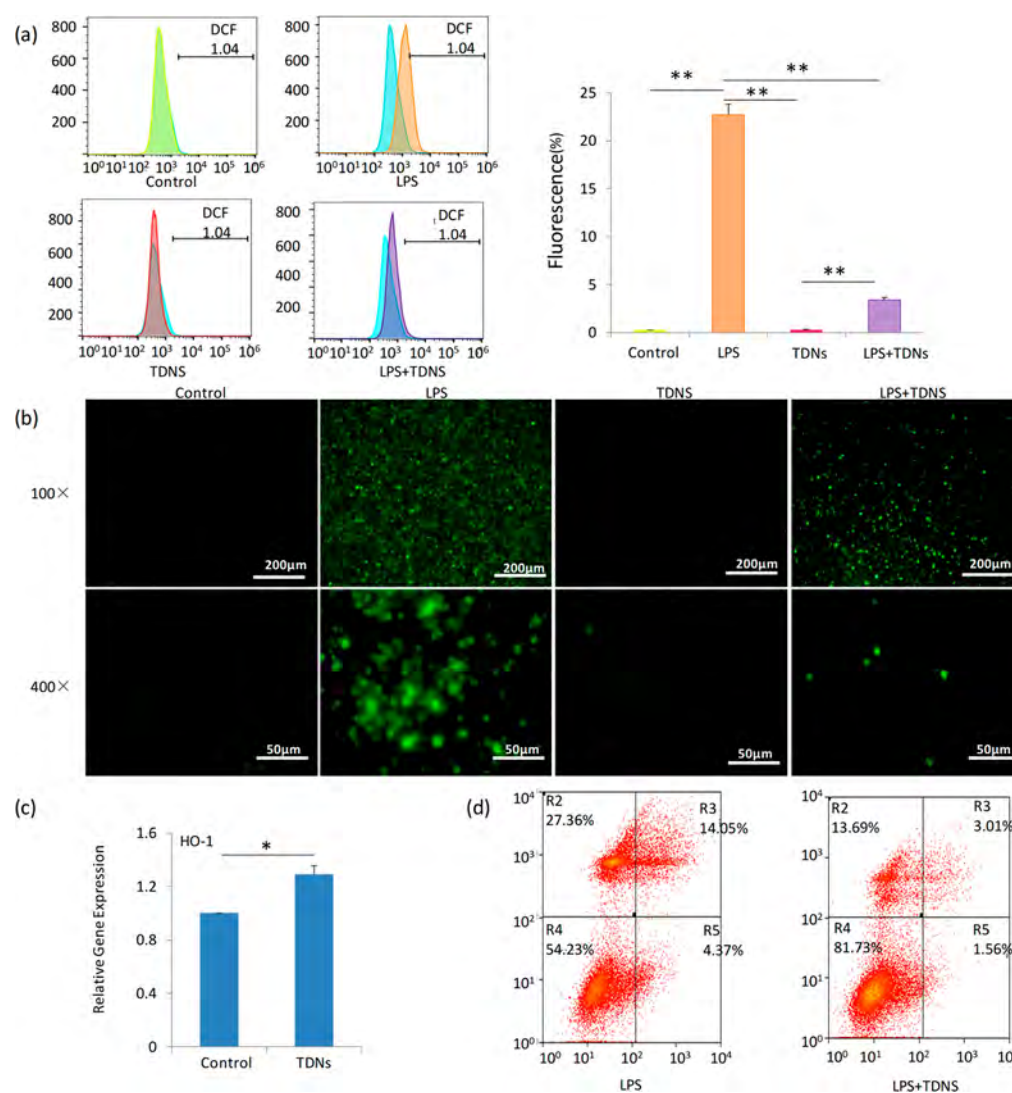


Figure 5. TDNs decreased ROS production in RAW264.7 cells. (a) Flow cytometric examination and analysis of intracellular ROS levels. Data are presented as mean \pm SD ($n = 4$). (b) Fluorescence microscope observation (100 \times and 400 \times) of intracellular ROS levels of treated RAW264.7 cells. (c) Q-PCR analysis of gene expressions of HO-1. Data are presented as mean \pm SD ($n = 4$). (d) Flow cytometric examination and analysis of apoptosis of cells subjected to LPS and LPS with TDNs. Statistical analysis: ** $p < 0.01$, * $p < 0.05$.

TDNs group (Figure 4b). In addition, we further confirmed our results via ELISA to detect some pro-inflammatory cytokines secreted by M1 macrophages. To rule out the possibility that the cytotoxicity of TDNs leads to the inhibition of the production of these cytokines, we normalized the results of ELISA by a CCK-8 assay (Supporting Information). It can be concluded from Figure 4c that pretreatment with TDNs resulted in decreased release of LPS-stimulated inflammatory cytokines (IL-1 β , IL-6, and TNF- α).

The function of M ϕ largely depends on their polarization, a process achieved by specific surface molecule upregulation and cytokine production. M1 macrophages can activate the tumor killing mechanism and enhance the Th1 immune response. Previous studies have suggested that accounting for the plasticity of M ϕ , an M2 ϕ to M1 ϕ macrophage polarization strategy may be useful for cancer immunotherapy.^{46,47} To the best of our knowledge, our present work is the first study reporting TDN-induced M1 polarization of RAW264.7 cells. It is worth mentioning that TDNs can cause a more moderate M1 polarization than that by LPS, which could avoid an excessive

inflammatory response. Therefore, it was revealed that TDNs are potentially useful candidates in immunomodulation.

3.5. TDNs Decrease ROS Production in RAW264.7 Cells. Oxidative stress refers to the production of intracellular ROS and antioxidant imbalance.⁴⁸ It leads to protein modification, lipid peroxidation, and subsequent cellular dysfunction⁴⁹ via the production of free radicals and is an important factor in aging and disease progression. To investigate whether TDNs play a role in antioxidative action, a fluorescence assay was developed by incorporating a DCFH-DA fluorescent probe into cells. Intracellular ROS can oxidize nonfluorescent DCFH to produce fluorescent DCF; the abundance of ROS can be determined based on green fluorescence emitted from the intracellular space. As shown in Figure 5a and b, LPS stimulated significantly improved intracellular ROS production compared to that of non-LPS controls. However, the ROS production induced by LPS was decreased by the application of TDNs, and TDNs had no significant effect on ROS production in the absence of LPS.

To further explore the mechanism underlying antioxidant activity of TDNs, the mRNA level of HO-1 was evaluated. The

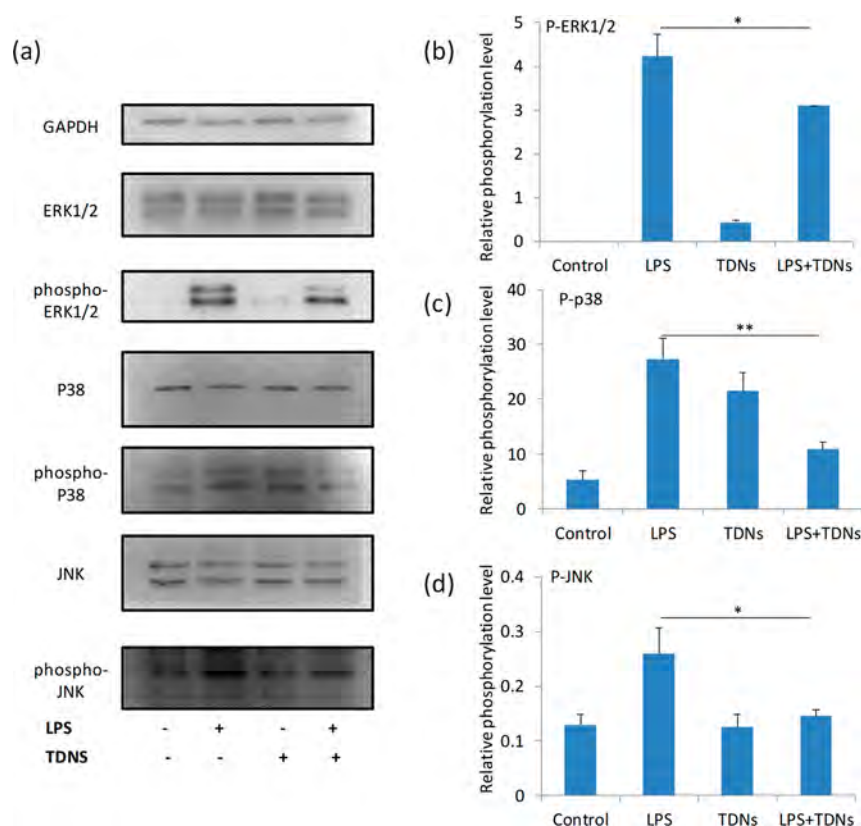


Figure 6. TDNs depressed LPS-induced phosphorylation of p38, ERK1/2, and JNK1/2/3 in RAW264.7 cells. (a) Western blot analysis of total ERK1/2, phospho-ERK1/2, total p38, phospho-p38, total JNK1/2/3, and phospho-JNK1/2/3 of RAW264.7 cells subjected to different treatments. (b–d) Quantification of phosphorylation level of p38, ERK1/2, and JNK. Data are presented as mean \pm SD ($n = 4$). Statistical analysis: * $p < 0.05$, ** $p < 0.01$. We specially labeled the statistic difference between the LPS group and LPS TDNs group.

results showed that the *HO-1* mRNA level in RAW264.7 cells was significantly upregulated after treatment with TDNs (Figure 5c). The antioxidative, antiapoptotic, and anti-inflammatory functions of protective *HO-1* have been widely studied,^{50,51} which may be due to the degradation of the antioxidant bilirubin or the coinduction of ferritin.^{52,53} Our results supported the protective effect of TDNs on RAW264.7 cells.

Moreover, as a regulator of apoptosis,⁵⁴ the significant upregulation of *HO-1* mRNA levels may indicate that apoptosis induction is associated with TDNs. To clarify this result, flow cytometry was employed. We used LPS to establish an inflammatory response model in RAW264.7 cells with or without TDN pretreatment. It can be summarized from Figure 5d that cell apoptosis exhibits significant changes 24 h after exposure to TDN. After TDN treatment, cells in the late phase of apoptosis dropped from 4.37% to 1.56%, those in the early phase of apoptosis dropped from 14.05% to 3.01%, and the dead cells decreased from 27.36% to 13.69%. In conclusion, TDNs attenuate apoptosis of RAW264.7 cells by upregulating *HO-1* expression.

Currently, potential therapeutic agents for antioxidative stress include antioxidative supplements, enzymes, nanoparticles, and NADPH oxidases.⁵⁵ They exert antioxidant effects by directly clearing or neutralizing ROS or by inhibiting the downstream adverse effects of ROS.⁵⁵ Taking advantage of their designability in structure, steady structure, sequence diversity, biocompatibility, biodegradable property, strong absorption capacity, and targeted delivery potential, TDNs exhibit better potency to reduce the dosage and side effects while maintaining

the function as imaging tracers and therapeutic agent carriers.^{4,56,57} In the future, the role of TDNs in the field of anti-inflammatory and antioxidative response can be expanded to targeted carriers of anti-inflammatory and antioxidative molecules, a Cy3/5-TDNs-based aptamer assay for filtrating macrophages with different polarization states, etc. They can also be applied to attenuate cell apoptosis and for therapy of aging and degenerative conditions without toxicity concerns associated with traditional nanoplateforms.

3.6. TDNs Suppress LPS-Induced MAPKs Phosphorylation in RAW264.7 Cells. In the inflammatory response, mitogen-activated protein kinase (MAPK) signaling has important effects on the regulation of pro-inflammatory cytokines and mediators. ERK1/2, JNK 1/2/3, and p38 are known as MAPK subfamilies.⁵⁸ In mammals, MAPKs comprise JNK, p38 MAPK, and ERK, and each of them exists in several isoforms.⁵⁹ MAPKs could upregulate multiple inflammation-related genes and regulate the inflammatory response. The JNK and p38 MAPK signaling pathways are activated by oxidative, genotoxic, and osmotic stresses as well as by microbial components.^{60,61} It was reported that myeloid cell-specific deletion of JNK1 and JNK2 could depress the expression of M1 macrophage-specific markers, which indicated that the JNK signaling pathway plays roles in pro-inflammatory pathways in macrophages.⁶² ERK could induce the production of TNF, IL-1 β , and IL-10 following TLR stimulation.⁶⁰ In addition, p38 α has important roles in activating feedback pathways that down-regulate inflammation.⁶³ To further elucidate the molecular pathways by which TDNs regulate macrophages to protect against oxidative stress and inflammation, the activations of

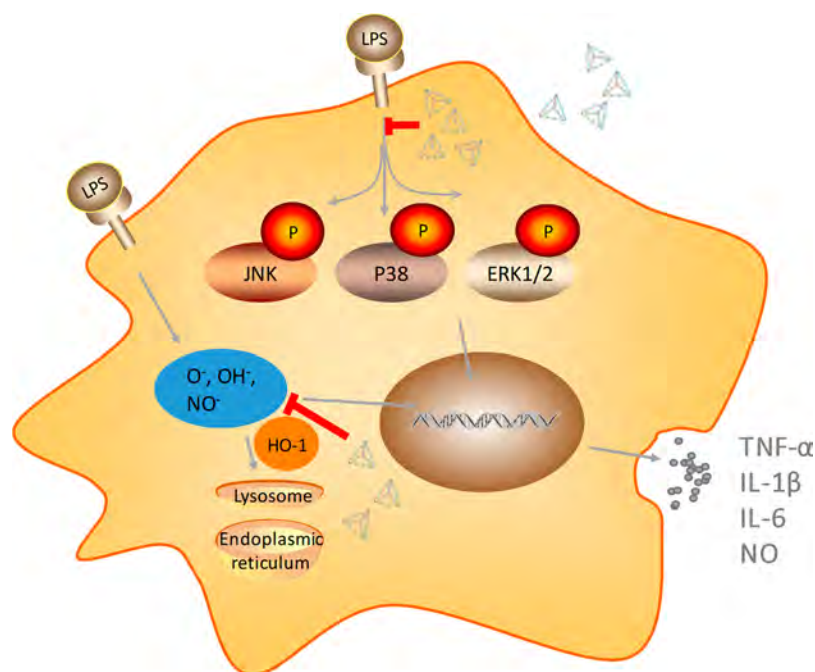


Figure 7. Cartoon representation of the anti-inflammation and combating oxidative stress effects of TDNs.

p38, ERK1/2, and JNK1/2/3 were examined by Western blotting (Figure 6a). In this study, LPS remarkably activated the MAPK subfamilies. However, activation of MAPK subfamilies (ERK, P38, and JNK) was downregulated by the application of TDNs (Figure 6b,c,d). In conclusion, TDNs protect macrophages from oxidative stress and inflammatory responses primarily by downregulating the LPS-induced phosphorylation of MAPK subfamilies (Figure 7).

4. CONCLUSIONS

To the best of our knowledge, this is the first study that comprehensively analyzes the immunological influences of TDNs, including the reaction to cell polarization and cell apoptosis as well as their anti-inflammatory and antioxidative effects. TDNs regulated oxidative stress and inflammation in macrophages via inhibiting the phosphorylation of MAPK subfamilies. Considering their good bioavailability and ease of targeting, TDNs have great potential as a novel theranostic agent for exhibiting anti-inflammatory and antioxidant activities.

■ ASSOCIATED CONTENT

Supporting Information

The Supporting Information is available free of charge on the ACS Publications website at DOI: 10.1021/acsami.7b17928.

CCK-8 results of RAW264.7 cells at 12 and 24 h after being treated with LPS and TDNs (PDF)

■ AUTHOR INFORMATION

Corresponding Author

*Tel.: 86-28-85503487. Fax: 86-28-85582167. E-mail: yunfenglin@scu.edu.cn.

ORCID

Yunfeng Lin: 0000-0003-1224-6561

Notes

The authors declare no competing financial interest.

■ ACKNOWLEDGMENTS

This work was funded by the National Natural Science Foundation of China (81671031, 81471803) and the Sichuan Science and Technology Innovation Team (2014TD0001).

■ REFERENCES

- (1) Tian, T.; Liao, J.; Zhou, T.; Lin, S.; Zhang, T.; Shi, S. R.; Cai, X.; Lin, Y. The Fabrication of Calcium Phosphate Microflowers and their Extended Application in Bone Regeneration. *ACS Appl. Mater. Interfaces* **2017**, *9*, 30437–30447.
- (2) Qu, X.; Wang, S.; Ge, Z.; Wang, J.; Yao, G.; Li, J.; Zuo, X.; Shi, J.; Song, S.; Wang, L.; Li, L.; Pei, H.; Fan, C. Programming Cell Adhesion for On-Chip Sequential Boolean Logic Functions. *J. Am. Chem. Soc.* **2017**, *139*, 10176–10179.
- (3) Qu, X.; Zhu, D.; Yao, G.; Su, S.; Chao, J.; Liu, H.; Zuo, X.; Wang, L.; Shi, J.; Wang, L.; Huang, W.; Pei, H.; Fan, C. An Exonuclease III-Powered, On-Particle Stochastic DNA Walker. *Angew. Chem., Int. Ed.* **2017**, *56*, 1855–1858.
- (4) Zhu, D.; Song, P.; Shen, J.; Su, S.; Chao, J.; Aldalbahi, A.; Zhou, Z.; Song, S.; Fan, C.; Zuo, X.; Tian, Y.; Wang, L.; Pei, H. PolyA-mediated DNA assembly on gold nanoparticles for thermodynamically favorable and rapid hybridization analysis. *Anal. Chem.* **2016**, *88*, 4949–4954.
- (5) Qu, X.; Zhang, H.; Chen, H.; Aldalbahi, A.; Li, L.; Tian, Y.; Weitz, D. A.; Pei, H. Convection Driven Pull-Down Assays in Nanoliter Droplets using Scaffolded Aptamers. *Anal. Chem.* **2017**, *89*, 3468–3473.
- (6) Chen, L.; Chao, J.; Qu, X.; Zhang, H.; Zhu, D.; Su, S.; Aldalbahi, A.; Wang, L.; Pei, H. Probing Cellular Molecules with PolyA-Based Engineered Aptamer Nanobeacon. *ACS Appl. Mater. Interfaces* **2017**, *9*, 8014–8020.
- (7) Farokhzad, O. C.; Langer, R. Impact of Nanotechnology on Drug Delivery. *ACS Nano* **2009**, *3*, 16–20.
- (8) Pei, H.; Zuo, X.; Pan, D.; Shi, J.; Huang, Q.; Fan, C. Scaffolded biosensors with designed DNA nanostructures. *NPG Asia Mater.* **2013**, *5*, e51–e60.
- (9) Wen, Y.; Pei, H.; Wan, Y.; Su, Y.; Huang, Q.; Song, S.; Fan, C. DNA nanostructure-decorated surfaces for enhanced aptamer-target binding and electrochemical cocaine sensors. *Anal. Chem.* **2011**, *83*, 7418–7423.

- (10) Zhou, G.; Lin, M.; Song, P.; Chen, X.; Chao, J.; Wang, L.; Huang, Q.; Huang, W.; Fan, C.; Zuo, X. Multivalent capture and detection of cancer cells with DNA nanostructured biosensors and multibranch hybridization chain reaction amplification. *Anal. Chem.* **2014**, *86*, 7843–7848.
- (11) Jiang, Q.; Song, C.; Nangreave, J.; Liu, X.; Lin, L.; Qiu, D.; Wang, Z. G.; Zou, G.; Liang, X.; Yan, H.; Ding, B. DNA origami as a carrier for circumvention of drug resistance. *J. Am. Chem. Soc.* **2012**, *134*, 13396–13403.
- (12) Peng, Q.; Shao, X. R.; Xie, J.; Shi, S. R.; Wei, X.; Zhang, T.; Cai, X.; Lin, Y. Understanding of the Biomedical Effects of the Self-assembled Tetrahedral DNA Nanostructure on Living Cells. *ACS Appl. Mater. Interfaces* **2016**, *8*, 12733–12739.
- (13) Tian, T.; Zhang, T.; Zhou, T.; Lin, S.; Shi, S.; Lin, Y. Synthesis of an ethyleneimine/tetrahedral DNA nanostructure complex and its potential application as a multi-functional delivery vehicle. *Nanoscale* **2017**, *9*, 18402–18412.
- (14) Li, Q.; Zhao, D.; Shao, X.; Lin, S.; Xie, X.; Liu, M.; Ma, W.; Shi, S.; Lin, Y. Aptamer-modified tetrahedral DNA nanostructure for tumor-targeted drug delivery. *ACS Appl. Mater. Interfaces* **2017**, *9*, 36695–36701.
- (15) Seeman, N. C. Nucleic acid junctions and lattices. *J. Theor. Biol.* **1982**, *99*, 237–247.
- (16) Lee, H.; Lyttonjean, A. K. R.; Chen, Y.; Love, K. T.; Park, A. I.; Karagiannis, E. D.; Sehgal, A.; Querbes, W.; Zurenko, C. S.; Jayaraman, M.; et al. Molecularly Self-Assembled Nucleic Acid Nanoparticles for Targeted In Vivo siRNA Delivery. *Nat. Nanotechnol.* **2012**, *7*, 389–393.
- (17) Walsh, A. S.; Yin, H.; Erben, C. M.; Wood, M. J.; Turberfield, A. J. DNA cage delivery to mammalian cells. *ACS Nano* **2011**, *5*, 5427–5432.
- (18) Li, J.; Pei, H.; Zhu, B.; Liang, L.; Wei, M.; He, Y.; Chen, N.; Li, D.; Huang, Q.; Fan, C. Self-Assembled Multivalent DNA Nanostructures for Noninvasive Intracellular Delivery of Immunostimulatory CpG Oligonucleotides. *ACS Nano* **2011**, *5*, 8783–8789.
- (19) Ge, Z.; Lin, M.; Wang, P.; Pei, H.; Yan, J.; Shi, J.; Huang, Q.; He, D.; Fan, C.; Zuo, X. Hybridization chain reaction amplification of microRNA detection with a tetrahedral DNA nanostructure-based electrochemical biosensor. *Anal. Chem.* **2014**, *86*, 2124–2130.
- (20) Shi, S.; Peng, Q.; Shao, X.; Xie, J.; Lin, S.; Zhang, T.; Li, Q.; Li, X.; Lin, Y. Self-Assembled Tetrahedral DNA Nanostructures Promote Adipose-Derived Stem Cell Migration via lncRNA XLOC 010623 and RHOA/ROCK2 Signal Pathway. *ACS Appl. Mater. Interfaces* **2016**, *8*, 19353–19363.
- (21) Shao, X.; Lin, S.; Peng, Q.; Shi, S.; Wei, X.; Zhang, T.; Lin, Y. *Small* **2017**, *13*, 1602770–1602781.
- (22) Shao, X. R.; Lin, S. Y.; Peng, Q.; Shi, S. R.; Li, X. L.; Zhang, T.; Lin, Y. F. Effect of tetrahedral DNA nanostructures on osteogenic differentiation of mesenchymal stem cells via activation of the Wnt/ β -catenin signaling pathway. *Nanomedicine* **2017**, *13* (5), 1809–1819.
- (23) Ye, F.; White, C. C.; Jin, Y.; Hu, X.; Hayden, S.; Zhang, X.; Gao, X.; Kavanagh, T. J.; Chiu, D. T. Toxicity and oxidative stress induced by semiconducting polymer dots in RAW264.7 mouse macrophages. *Nanoscale* **2015**, *7*, 10085–10093.
- (24) Su, L.; Zhang, W.; Wu, X.; Zhang, Y.; Chen, X.; Liu, G.; Chen, G.; Jiang, M. Glycocalyx-Mimicking Nanoparticles for Stimulation and Polarization of Macrophages via Specific Interactions. *Small* **2015**, *11*, 4191–4200.
- (25) Fu, N.; Liao, J.; Lin, S.; Sun, K.; Tian, T.; Zhu, B.; Lin, Y. PCL-PEG-PCL film promotes cartilage regeneration in vivo. *Cell Proliferation* **2016**, *49*, 729–739.
- (26) Liao, J.; Tian, T.; Shi, S.; Xie, X.; Ma, Q.; Li, G.; Lin, Y. The fabrication of biomimetic biphasic CAN-PAC hydrogel with a seamless interfacial layer applied in osteochondral defect repair. *Bone Res.* **2017**, *5*, 137–151.
- (27) Zhang, T.; Gong, T.; Xie, J.; Lin, S.; Liu, Y.; Zhou, T.; Lin, Y. Softening Substrates Promote Chondrocytes Phenotype via RhoA/ROCK Pathway. *ACS Appl. Mater. Interfaces* **2016**, *8*, 22884–22891.
- (28) Zhong, J.; Guo, B.; Xie, J.; Deng, S.; Fu, N.; Lin, S.; Li, G.; Lin, Y.; Cai, X. Crosstalk between adipose-derived stem cells and chondrocytes: when growth factors matter. *Bone Res.* **2016**, *4*, 15036–15046.
- (29) Gong, T.; Xie, J.; Liao, J.; Zhang, T.; Lin, S.; Lin, Y. Nanomaterials and bone regeneration. *Bone Res.* **2015**, *3*, 15029–15035.
- (30) Zhang, T.; Lin, S.; Shao, X.; Zhang, Q.; Xue, C.; Zhang, S.; Lin, Y.; Zhu, B.; Cai, X. Effect of matrix stiffness on osteoblast functionalization. *Cell Proliferation* **2017**, *50*, e12338–12346.
- (31) Zhou, T.; Li, G.; Lin, S.; Tian, T.; Ma, Q.; Zhang, Q.; Shi, S.; Xue, C.; Ma, W.; Cai, X.; Lin, Y. Electrospun Poly (3-Hydroxybutyrate-Co-4-Hydroxybutyrate)/Graphene Oxide Scaffold: Enhanced Properties and Promoted in Vivo Bone Repair in Rats. *ACS Appl. Mater. Interfaces* **2017**, *9*, 42589–42600.
- (32) Xue, C.; Xie, J.; Zhao, D.; Lin, S.; Zhou, T.; Shi, S.; Shao, X.; Lin, Y.; Zhu, B.; Cai, X. The JAK/STAT3 signalling pathway regulated angiogenesis in an endothelial cell/adipose-derived stromal cell coculture, 3D gel model. *Cell Proliferation* **2017**, *50*, 12307–12316.
- (33) Zhang, Q.; Lin, S.; Zhang, T.; Tian, T.; Ma, Q.; Xie, X.; Xue, C.; Lin, Y.; Zhu, B.; Cai, X. Curved microstructures promote osteogenesis of mesenchymal stem cells via the RhoA/ROCK pathway. *Cell Proliferation* **2017**, *50*, 12356–12365.
- (34) Han, G.; Ghosh, P.; Rotello, V. M. Functionalized gold nanoparticles for drug delivery. *Nanomedicine* **2007**, *2*, 113–123.
- (35) Ouyang, X.; Li, J.; Liu, H.; Zhao, B.; Yan, J.; He, D.; Fan, C.; Chao, J. Self-assembly of DNA-based drug delivery nanocarriers with rolling circle amplification. *Methods* **2014**, *67*, 198–204.
- (36) Shi, S.; Lin, S.; Shao, X.; Li, Q.; Tao, Z.; Lin, Y. Modulation of chondrocyte motility by tetrahedral DNA nanostructures. *Cell Proliferation* **2017**, *50*, e12368–12376.
- (37) Liang, L.; Li, J.; Li, Q.; Huang, Q.; Shi, J.; Yan, H.; Fan, C. Single-Particle Tracking and Modulation of Cell Entry Pathways of a Tetrahedral DNA Nanostructure in Live Cells. *Angew. Chem., Int. Ed.* **2014**, *53*, 7745–7750.
- (38) Fry, N. L.; Mascharak, P. K. Photoactive ruthenium nitrosyls as NO donors: how to sensitize them toward visible light. *Acc. Chem. Res.* **2011**, *44*, 289–298.
- (39) Liu, Z.; Li, W.; Wang, F.; Sun, C.; Wang, L.; Wang, J.; Sun, F. Enhancement of lipopolysaccharide-induced nitric oxide and interleukin-6 production by PEGylated gold nanoparticles in RAW264.7 cells. *Nanoscale* **2012**, *4*, 7135–7142.
- (40) Xiang, H. J.; Guo, M.; Liu, J. G. Transition-Metal Nitrosyls for Photocontrolled Nitric Oxide Delivery. *Eur. J. Inorg. Chem.* **2017**, *2017*, 1586–1595.
- (41) Elsehemy, A.; Postovit, L. M.; Fu, Y. Nitric oxide signaling in human ovarian cancer: A potential therapeutic target. *Nitric Oxide* **2016**, *54*, 30–37.
- (42) Dey, D.; Chaskar, S.; Athavale, N.; Chitre, D. Inhibition of LPS Induced TNF α and NO Production in Mouse Macrophage and Inflammatory Response in Rat Animal Models by a Novel Ayurvedic Formulation, BV-9238. *Phytother. Res.* **2014**, *28*, 1479–1485.
- (43) Grabowski, P. S.; Macpherson, H.; Ralston, S. H. Nitric oxide production in cells derived from the human joint. *Rheumatology* **1996**, *35*, 207–212.
- (44) Sierra, A.; Navascués, J.; Cuadros, M. A.; Calvente, R.; Martín-Oliva, D.; Ferrer-Martín, R. M.; Martín-Estebané, M.; Carrasco, M. C.; Marín-Teva, J. L. Expression of Inducible Nitric Oxide Synthase (iNOS) in Microglia of the Developing Quail Retina. *PLoS One* **2014**, *9*, e106048–106063.
- (45) D'Alessio, F. R.; Tsushima, K.; Aggarwal, N. R.; Mock, J. R.; Eto, Y.; Garibaldi, B. T.; Files, D. C.; Avalos, C. R.; Rodriguez, J. V.; Waickman, A. T.; et al. Resolution of experimental lung injury by monocyte-derived inducible nitric oxide synthase. *J. Immunol.* **2012**, *189*, 2234–2245.
- (46) Su, L.; Zhang, W.; Wu, X.; Zhang, Y.; Chen, X.; Liu, G.; Chen, G.; Jiang, M. Glycocalyx-Mimicking Nanoparticles for Stimulation and Polarization of Macrophages via Specific Interactions. *Small* **2015**, *11*, 4191–4120.

(47) Bingle, L.; Brown, N. J.; Lewis, C. E. The role of tumour-associated macrophages in tumour progression: implications for new anticancer therapies. *J Pathol* 196:254–265. *J. Pathol.* **2002**, *196*, 254–265.

(48) Song, D.; Cheng, Y.; Li, X.; Wang, F.; Lu, Z.; Xiao, X.; Wang, Y. Biogenic nano-selenium particles effectively attenuate oxidative stress-induced intestinal epithelial barrier injury by activating the Nrf2 antioxidant pathway. *ACS Appl. Mater. Interfaces* **2017**, *9*, 14724–14740.

(49) Čáp, M.; Váňová, L.; Palková, Z. Reactive Oxygen Species in the Signaling and Adaptation of Multicellular Microbial Communities. *Oxid. Med. Cell. Longevity* **2012**, *2012*, 976753–976765.

(50) Abraham, N. G.; Kappas, A. Pharmacological and clinical aspects of heme oxygenase. *Pharmacol. Rev.* **2008**, *60*, 79–127.

(51) Zheng, M.; Kim, S. K.; Joe, Y.; Back, S. H.; Cho, H. R.; Kim, H. P.; Ignarro, L. J.; Chung, H. T. Sensing endoplasmic reticulum stress by protein kinase RNA-like endoplasmic reticulum kinase promotes adaptive mitochondrial DNA biogenesis and cell survival via heme oxygenase-1/carbon monoxide activity. *FASEB J.* **2012**, *26*, 2558–2568.

(52) Durante, W. Targeting heme oxygenase-1 in vascular disease. *Curr. Drug Targets* **2010**, *11*, 1504–1516.

(53) Maamoun, H.; Zachariah, M.; Mcvey, J. H.; Green, F. R.; Agouni, A. Heme oxygenase (HO)-1 induction prevents Endoplasmic Reticulum stress-mediated endothelial cell death and impaired angiogenic capacity. *Biochem. Pharmacol.* **2017**, *127*, 46–59.

(54) Mylroie, H.; Dumont, O.; Bauer, A.; Thornton, C. C.; Mackey, J.; Calay, D.; Hamdulay, S. S.; Choo, J. R.; Boyle, J. J.; Samarel, A. M.; Randi, A. M.; Evans, P. C.; Mason, J. C. PKC ϵ -CREB-Nrf2 signalling induces HO-1 in the vascular endothelium and enhances resistance to inflammation and apoptosis. *Cardiovasc. Res.* **2015**, *106*, 509–519.

(55) Li, T.; Xiao, L.; Yang, J.; Ding, M.; Zhou, Z.; Laconte, L.; Jin, L.; Dorn, H. C.; Li, X. Trimetallic Nitride Endohedral Fullerenes Carboxyl-Gd₃N@C₈₀: A New Theranostic Agent for Combating Oxidative Stress and Resolving Inflammation. *ACS Appl. Mater. Interfaces* **2017**, *9*, 17681–17687.

(56) Yang, X.; Li, J.; Pei, H.; Li, D.; Zhao, Y.; Gao, J.; Lu, J.; Shi, J.; Fan, C.; Huang, Q. Pattern Recognition Analysis of Proteins Using DNA-Decorated Catalytic Gold Nanoparticles. *Small* **2013**, *9*, 2844–2849.

(57) Chen, Q.; Liu, H.; Lee, W.; Sun, Y.; Zhu, D.; Pei, H.; Fan, C.; Fan, X. Self-assembled DNA tetrahedral optofluidic lasers with precise and tunable gain control. *Lab Chip* **2013**, *13*, 3351–3354.

(58) Johnson, G. L.; Lapadat, R. Mitogen-Activated Protein Kinase Pathways Mediated by ERK, JNK, and p38 Protein Kinases. *Science* **2002**, *298*, 1911–1912.

(59) Kim, E. K.; Choi, E. J. Compromised MAPK signaling in human diseases: an update. *Arch. Toxicol.* **2015**, *89*, 867–882.

(60) Tai, C. J.; Chang, S. J.; Leung, P. C.; Tzeng, C. R. ATP activates nuclear translocation of mitogen-activated protein kinases in human granulosa-luteal cells. *Fertil. Steril.* **2004**, *82*, S302.

(61) Sabio, G.; Davis, R. J. TNF and MAP kinase signalling pathways. *Semin. Immunol.* **2014**, *26*, 237–245.

(62) Martinez, F. O.; Helming, L.; Gordon, S. Alternative activation of macrophages: an immunologic functional perspective. *Annu. Rev. Immunol.* **2009**, *27*, 451–483.

(63) Kim, C.; Sano, Y.; Todorova, K.; Carlson, B. A.; Arpa, L.; Celada, A.; Lawrence, T.; Otsu, K.; Brissette, J. L.; Arthur, J. S. C.; Park, J. M. The kinase p38 alpha serves cell type-specific inflammatory functions in skin injury and coordinates pro- and anti-inflammatory gene expression. *Nat. Immunol.* **2008**, *9*, 1019–1027.